Dynamic Flow in a Kenics Static Mixer: An Assessment of Various CFD Methods

W. F. C. van Wageningen, D. Kandhai, R. F. Mudde, and H. E. A. van den Akker
Kramers Laboratorium voor Fysische Technologie, Faculty of Applied Physics, Delft University of Technology, Prins Bernhardlann 6, 2628 BW Delft, The Netherlands

DOI 10.1002/aic.10178
Published online in Wiley InterScience (www.interscience.wiley.com).

The flow in the Kenics static mixer is investigated in detail both numerically and experimentally in the range of Re = 100· · ·1000. It was found that at Re = 300 the flow becomes unsteady. Two numerical methods, the lattice Boltzmann (LB) method and FLUENT, were compared and used to simulate the flow. The LB method proved to be a relatively fast and cheap (in terms of memory) alternative for the simulation of the transient flow in the Kenics static mixer at Re > 300. Furthermore, the flow field and dynamic behavior were validated by means of LDA experiments. The transient behavior observed could be explained by studying the dynamics of the vortices in the flow. The transition to unsteady flow takes place, when the vortices start to stretch out over an entire mixing element and create a disturbance in the flow, which subsequently triggers the unsteady behavior. © 2004 American Institute of Chemical Engineers *AIChE J,* 50: 1684–1696, 2004

Keywords: Kenics static mixer, FLUENT, lattice Boltzmann (LB), computational fluid dynamics (CFD), laser Doppler anemometry (LDA), oscillation, vortex

Introduction

The Kenics static mixer, designed in the 1960s, is mainly used for in-line blending of liquid, heat exchange, and to promote plug flow (that is, uniform residence time). The numerous studies conducted over the past decades focus on one or more of these three research topics.

(1) The publications that focus on mixing are Grace (1971), Wilkinson and Cliff (1977), Sir and Lecjacks (1982), Pahl and Muschelknautz (1982), Heywood et al. (1984), Arimond and Erwin (1985), Bakker and LaRoche (1995), Rauline et al. (1995, 2000), Hobbs and Muzzio (1997a, 1998), and Hobbs et al. (1998).

(2) The publications that focus on heat exchange are Grace (1971), Chen and MacDonald (1973), Genetti (1982), Cybulski and Werner (1986), Lecjacks et al. (1987), and Joshi et al. (1995).

(3) The publications that focus on the residence time distribution are Grace (1971), Nigam et al. (1980), Kemblowski and Pustelnik (1988), and Hobbs and Muzzio (1997b).

There are several advantages that a static mixer has over a mechanical mixer (such as a stirred tank reactor): the low maintenance and operating costs, low space requirements, and the fact that there are no moving parts in a static mixer. A static mixer is in principle nothing more than a stationary obstacle placed in a tubular reactor to promote mixing. In the case of the Kenics static mixer the obstacle consists of twisted metal plates, which are welded together. The twisted plates or mixing elements are designed in such a way that a mixing element splits the liquid into two streams and recombines the two streams formed by the previous element. This is achieved by placing the elements at an angle of 90°. The twist angle of a mixing element is 180° and two consecutive elements alternate in rotation direction (see Figure 1). This way the liquid is not only split at each element, but also forced to change its rotation, which also contributes to the mixing by the formation of vortices and "stretching" of the fluid. More information about static mixers can be found in Harnby et al. (1992).

Correspondence concerning this article should be addressed to W. F. C. van Wageningen at nielsvw@klft.tn.tudelft.nl.

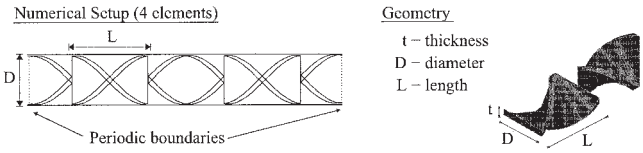

Figure 1. Numerical setup and geometry of Kenics static mixer.

Here, the Kenics static mixer is investigated as part of a project that concerns the recovery of copper from waste streams by means of waste-to-waste technology (Hage et al., 1999). Waste-to-waste technology is based on cleaning waste streams by combining two different waste streams. In this project waste streams containing copper ions are combined with waste streams containing carbohydrates to recover copper particles, which constitute the end product. The copper particles formed grow during their residence in the reactor and their size determines their economic value. A more uniform size has a higher economic value. Therefore, to improve the economic value of the end product, it is important to control the residence time of the copper particles. One way to achieve this is to place Kenics static mixers along the reactor.

One of the problems that can occur in the Kenics static mixer reactor is the entrapment of particles. To keep all particles in suspension a high velocity—and as a result a high Reynolds number (Re $\approx 10^5$)—is necessary. However, the growth of the particles is a slow process, which leads together with the high axial velocity to an extremely long reactor. Therefore, as an alternative, a vertical reactor is investigated. The vertical reactor avoids problems with sedimentation and can operate at much lower velocities. The only restrictions are the residence time distribution and the mixing of the particles, which both have to be virtually uniform. The Reynolds number at which such a reactor should operate varies from $Re = 100$ to $Re = 1000$. For this range little is known about the laminar structures that occur in the flow of a Kenics static mixer because most studies present reliable data only on low Reynolds number flows ($Re < 10$) [for example, Hobbs et al. (1998) and Bakker and LaRoche (1995), who both used FLUENT to simulate the flow in the Kenics static mixer].

Unfortunately, validation is often lacking in the literature, whereas a good grid independence study or comparison with experiments is a vital part of computational fluid dynamics (CFD). Therefore, CFD results that were obtained at a relatively high Reynolds number ($Re > 200$) and on a relatively coarse grid (for example, Hobbs and Muzzio, 1998) should be interpreted with care and it can be questioned whether all the results are valid. Thus, the aim of this study is to obtain accurate results up to at least $Re = 500$ and to validate these results with LDA measurements for the flow in a Kenics static mixer.

In the literature several numerical studies on the flow in a Kenics static mixer have been published. The focus was either on the pressure drop (Rauline et al., 1995) or the mixing characteristics (Arimond and Erwin 1985; Hobbs and Muzzio, 1997a,b), which are to a large extent based on the work of Ottino (1989). Arimond and Erwin (1985) were among the first to study the mixing properties of the Kenics static mixer with CFD. They simulated the mixing of two similar fluids, which differed only in color (black and white), and they showed that their results are in good agreement with a comparable experiment. Hobbs and Muzzio (1997a,b) used the commercial finite-volume (FV) code FLUENT to calculate the flow field and developed software to track tracer particles through the static mixer to characterize the mixing. This approach was also followed by Fourcade et al. (2001), who used a finite-element (FE) code, POLY3D, to calculate the flow field and an in-house code to track the tracer particles. Fourcade et al. (2001) validated the mixing characteristics of the static mixers by means of laser-induced fluorescence (LIF).

To track small particles in the static mixer, Mudde et al. (2002) solved the particle force balance, in which only the drag force was considered. They showed that the end location of a particle is very sensitive to small errors in its trajectory. Their explanation is that a particle has to chose either "left" or "right," when it approaches a new mixing element. Therefore, small errors in the particle trajectory can cause a different "choice" at one of the elements, which will lead to a totally different end position of the particle. A similar argument can be made for the flow field. Small errors in the flow field might, therefore, also lead to different trajectories of the particles, which stresses the importance of an accurate flow field and the need for validation. One should note that this argumentation is valid for a single particle realization and that despite the large errors, which can be made in a single realization, the statistical information obtained with multiple particle realizations can still be correct.

In this investigation the commercial package FLUENT was used to calculate the flow in the Kenics static mixer. FLUENT is a generic multipurpose code, which can be applied with success to various applications (Fluent Inc., 2003a). However, in an attempt to refine the computational grid used in the Kenics static mixer, FLUENT appeared to have very high memory requirements for the refined mesh, which was ultimately needed for the grid independence tests at relatively high Reynolds numbers ($Re = 500$). Therefore, an alternative approach was used: the lattice Boltzmann (LB) method. Kandhai et al. (1999) showed that LB could be used to simulate the flow in an SMRX static mixer and can be an alternative for standard (FV) or (FE) codes. However, in their work a detailed validation with an experimentally measured flow field was not reported. Furthermore, the geometry of the SMRX static mixer is very different from the Kenics static mixer considered in this work.

This communication will describe the comparison of the performance of the commercial package FLUENT V6 (FV) to the LB code with respect to CPU time and memory requirements, and will give an overview of the grid-independent CFD results of different flow regimes, which occur in the Kenics static mixer. The CFD results are validated by means of laser Doppler anemometry (LDA) measurements. Furthermore, the transition from steady to unsteady flow at $Re \approx 300$ is investigated in detail both experimentally and numerically. In the next section, the numerical methods (LB and FLUENT) are described and a validation of both methods is shown. In the third section, the LDA setup is described and the LDA results are compared with the LB results. Finally, the dynamic behavior in the Kenics static mixer is discussed in more detail and the conclusions are presented.

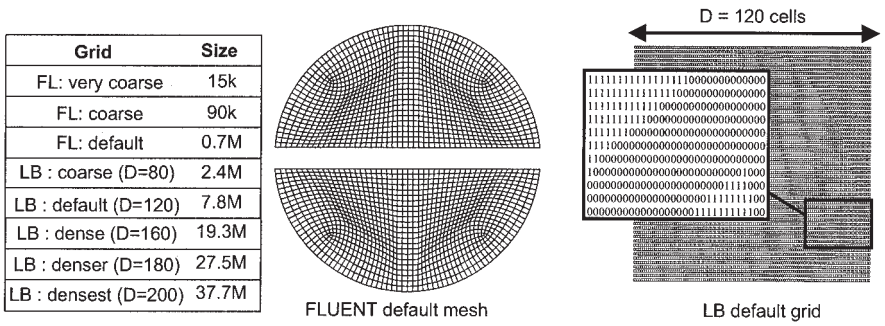

Figure 2. Overview of cross sections of grids used.

Computation of Flow Field

Numerical setup

The commercial package FLUENT V6 and an in-house lattice Boltzmann code (LB) are used to simulate the flow in a four-element Kenics static mixer. The aspect ratios of the mixing elements are $t/D = 0.08$ and $L/D = 1.5$ (see Figure 1). Periodic boundary conditions and a constant body force are applied in the axial direction and no slip boundaries are used at the wall. This way an "infinitely" long mixer is simulated. The FLUENT grid is created with GAMBIT 2.0 and consists of 700K hexahedral cells twisted along the elements. The (structured and staircased) LB grid consists of 10M grid nodes, which decreases to 7.8M nodes in the flow domain. The other nodes are wall nodes. The different grids are illustrated in Figure 2. Different cases are solved on a Linux (Redhat 7.1) cluster with multiple nodes. Each node has a dual Intel Pentium processor (2 times 1.6 GHz) and 1 GB of memory. All simulations are carried out on two nodes (4 CPUs, 2 GB). An overview of the interpolation schemes and solver options used in FLUENT and a more detailed description of the LB method are given in the next section.

Different Reynolds numbers ($Re = 10 \cdots 1000$), which are based on the tube diameter D and mean axial velocity $\bar{u}_{ax}$ are investigated. The Reynolds number is adjusted by varying the viscosity η of the liquid. The initial condition of the simulated flow in the mixer is a zero velocity field, on which a constant body force, F_b, is applied (similar to gravity). Eventually, the flow converges to a certain pressure drop and mean axial velocity, which determines the Reynolds number. For $Re < 200$ the flow converges to a steady-state solution, whereas for $Re > 300$ the flow remains unsteady. Figure 3 shows the mean axial velocity, which is developing from startup at $Re = 500$. The mean axial velocity is made dimensionless by its average value in the time interval 9,000 to 10,000 LB s. (LB s indicates the time in lattice Boltzmann units.) The small fluctuations in the mean axial velocity indicate the unsteady behavior and are observed in both the FLUENT and LB simulations. A small time step is necessary to capture these oscillations, which is by definition 1 LB s for the LB simulation and is set to 10 LB s for the FLUENT simulation.

LB solver

In contrast to conventional numerical schemes, which are based on discretizations of the macroscopic continuum equations, the lattice Boltzmann method is a mesoscopic approach for simulating fluid flow. In this method a fluid is modeled by the dynamics of the population of fictitious particles, which reside on a discrete lattice. The lattice nodes are linked with a number of their neighbors. In the case of the D3Q19 BGK (Bhatnagar–Gross–Krook) model (Qian et al., 1992), which is used in this study, each node has 18 links to neighboring nodes (remaining particles are also included at each node). The particles move along these links during the propagation phase and interact with each other during the so-called collision phase, in which the particles exchange momentum by a specific collision operator. In the BGK model the collision operator is based on

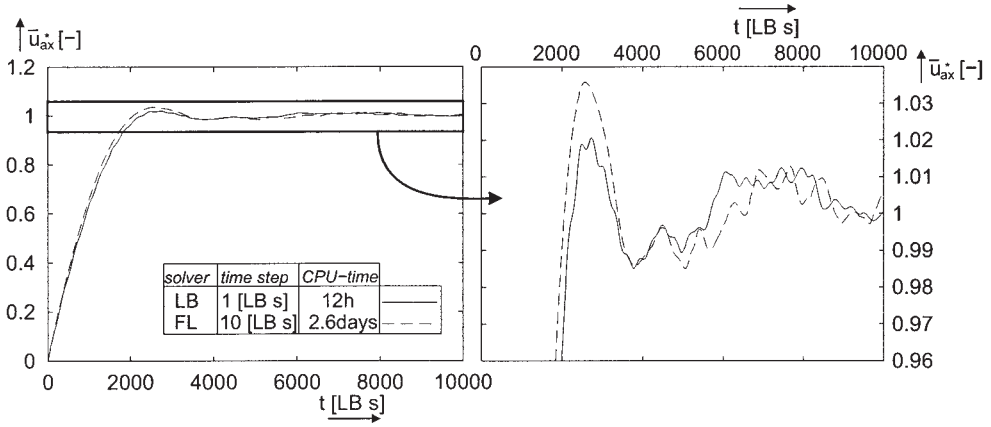

Figure 3. Development of mean axial velocity at $Re = 200$ from startup ($t = 0$, $\vec{u} = 0$) on the default grids.

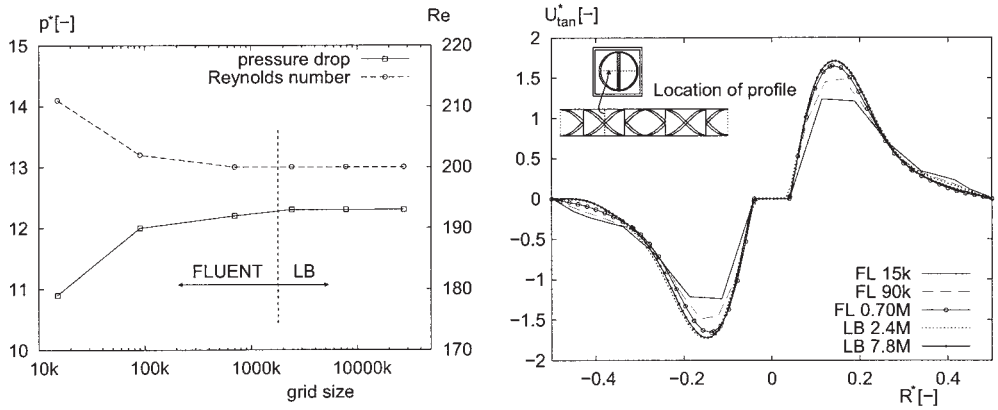

Figure 4. Grid independence check of pressure drop, Reynolds number, and tangential velocity profiles around *Re* = 200 at *t* = 10,000 LB s.

a single time relaxation. The time evolution of the BGK model is given by the following equation

$$f_i(\mathbf{r} + \mathbf{c}_i, t + 1) = f_i(\mathbf{r}, t) + \frac{1}{\tau}[f_i^{\text{eq}}(\mathbf{r}, t) - f_i(\mathbf{r}, t)] \quad (1)$$

where $f_i(\mathbf{r}, t)$ denotes the particle density that resides on lattice point $\mathbf{r}$ at time step t, and is moving along link i with local particle velocity $\mathbf{c}_i$; τ is the so-called BGK relaxation parameter. The equilibrium distribution function f_i^{eq} (valid for small Mach numbers) can be written up to $O(\mathbf{u}^2)$ (Qian et al., 1992)

$$f_i^{\text{eq}} = \rho w_i\left[1 + 3\mathbf{c}_i\mathbf{u} + \frac{9}{2}(\mathbf{c}_i \cdot \mathbf{u})^2 - \frac{3}{2}\mathbf{u}^2\right] \quad (2)$$

where ρ is the density, w_i are the weight factors, and $\mathbf{u}$ is the macroscopic velocity (in LB units). The density and macroscopic velocity can be obtained at each lattice point from the moments of the distribution function $f_i(\mathbf{r}, t)$

$$\rho(\mathbf{r}, t) = \sum_{i=0}^{18} f_i(\mathbf{r}, t) \quad (3)$$

$$\mathbf{u}(\mathbf{r}, t) = \frac{\sum_{i=0}^{18} f_i(\mathbf{r}, t)\mathbf{c}_i}{\rho(\mathbf{r}, t)} \quad (4)$$

The pressure is linked to the density and is equal to $p = \rho/3$. Qian and Orszag (1993) showed that if the density variation $\delta\rho$ is small, the corresponding momentum equation is the same as the Navier–Stokes equation (in LB units). A detailed overview of the lattice Boltzmann method can be found in Chen and Doolen (1998).

The LB method uses a staircase, structured grid and as a result a large number of grid points are necessary. The grid spacing determines the time-step size. Therefore, a dense grid will lead to a small time step. The tube diameter in LB units is equal to the number of nodes in the radial direction, $n_{\text{nodes,rad}}$, and the viscosity is equal to $\eta = (2\tau - 1)/6$. The body force was equal to $F_b = 10^{-4}$ and τ was used to set the viscosity. The Reynolds number can be used to scale and is given by

$$\text{Re} = \frac{6\rho n_{\text{nodes,rad}}\bar{u}_{\text{ax}}}{2\tau - 1} \quad (5)$$

The LB units can be transformed to dimensionless units in the following way

$$\rho^* = 1 \qquad D^* = 1 \qquad \overline{u^*}_{\text{ax}} = 1 \qquad \eta^* = \frac{1}{\text{Re}}$$

$$l^* = \frac{l}{n_{\text{nodes,rad}}} \qquad u^* = \frac{u}{\bar{u}_{\text{ax}}} \qquad t^* = \frac{tn_{\text{nodes,rad}}}{\bar{u}_{\text{ax}}} \qquad p^* = \frac{\frac{p}{3} - F_b x}{\rho \cdot \bar{u}_{\text{ax}}^2}$$

where the symbol * is used to denote the dimensionless units. The "LDA" units can be transformed to dimensionless units in a similar manner

$$\text{Re} = \frac{\rho_0 D_0 \bar{u}_{0,\text{ax}}}{\eta_0}$$

$$\rho^* = 1 \qquad D^* = 1 \qquad \overline{u^*}_{\text{ax}} = 1 \qquad \eta^* = \frac{1}{\text{Re}}$$

$$l^* = \frac{l}{D_0} \qquad u^* = \frac{u}{\bar{u}_{0,\text{ax}}} \qquad t^* = \frac{tD_0}{\bar{u}_{0,\text{ax}}} \qquad p^* = \frac{p_0}{\rho_0 \cdot \bar{u}_{0,\text{ax}}^2}$$

where the subscript 0 denotes the values used in the LDA experiment.

FLUENT solver

FLUENT is a generic multipurpose code for modeling fluid flow and heat transfer in complex geometries. It numerically solves the Navier–Stokes equations on unstructured meshes. The Navier–Stokes equation for a Newtonian fluid yields

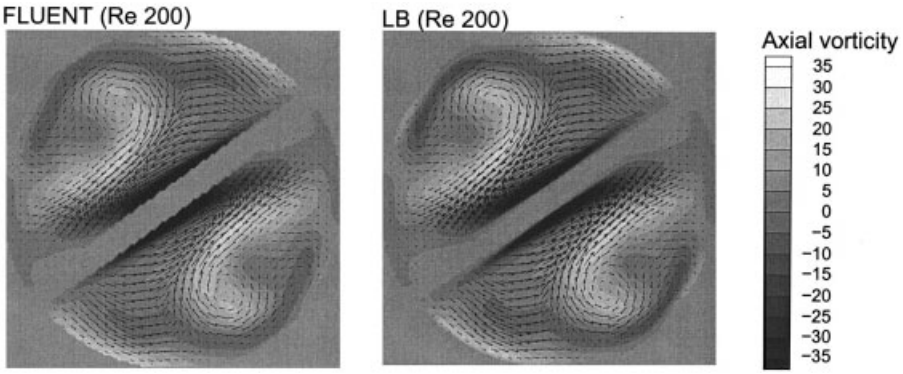

Figure 5. Flow structures and vorticity at *Re* = 200 on the default FLUENT and LB grids.

Located at $0.3D$ from the start of mixing element and at t = 10,000 LB s.

$$\frac{\partial \mathbf{u}}{\partial t} + \mathbf{u} \cdot \nabla \mathbf{u} = -\frac{1}{\rho} \nabla p + \frac{\eta}{\rho} \nabla^2 \mathbf{u} \tag{6}$$

A detailed description of the solver and interpolation schemes that are used by FLUENT can be found in Fluent Inc. (2003b).

For the sake of simplicity the FLUENT parameters are matched to the LB parameters and the solution was obtained in LB units. The LB units are translated to dimensionless units afterward. For this specific application the following solver options were selected in FLUENT:

- The segregated solver with second-order implicit temporal discretization
- The central-differencing discretization scheme (CDS)
- The second-order pressure scheme

The equations were interpolated until convergence was reached within one time step (10^{-3} for continuity, 10^{-4} for velocities).

Grid independence and pressure drop

Results obtained on different grid sizes are compared, which have a size of 15K, 90K, and 700K for the FLUENT solver and 2.4M, 7.8M, 19.3M, 27.5M, and 37.7M for the LB solver, respectively. The results corresponding to Re = 200 and Re = 500, respectively, are compared with respect to the pressure drop, velocity, and vorticity. The LB results are used as a reference point for the FLUENT results.

The lefthand side of Figure 4 shows the pressure drop and Reynolds number at different grid sizes and at t = 10,000 LB s. The Reynolds number is determined by the average axial velocity, to which the solution eventually converges. The viscosity and body force are set in such a way that a Reynolds number of Re = 200 is obtained. The points to the right are calculated with the LB method, whereas the others are calculated with FLUENT. It should be noted that because all the simulations have the same initial conditions, they should converge to the same Reynolds number and pressure drop. The right-hand side of Figure 4 shows the corresponding velocity profiles that are located along a line halfway along a mixing element.

It can be observed that the pressure drop and Reynolds number can already be predicted with reasonable accuracy at a relatively coarse (90K) FLUENT mesh. However, the corresponding velocity profile obtained on this mesh still shows some differences with the ones obtained on the more dense meshes. On the other hand, the velocity profile obtained on the default FLUENT mesh compares reasonably well to the velocity profiles obtained on the 2.4M and 7.8M LB grids. So, to obtain accurate results for Re = 200, the minimal requirements

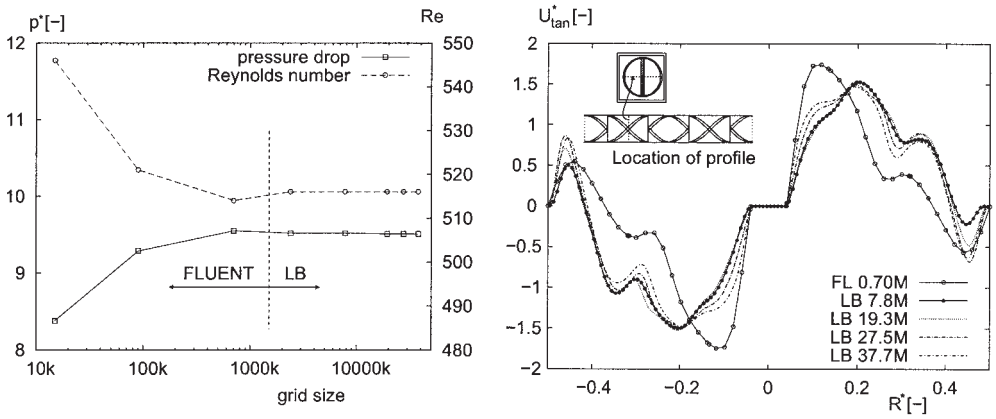

Figure 6. Grid independence check of pressure drop, Reynolds number, and tangential velocity profiles around *Re* = 500 at *t* = 10,000 LB s.

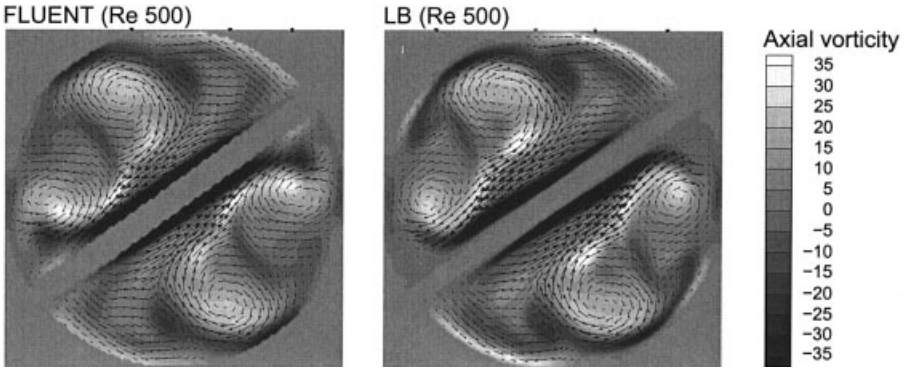

Figure 7. Flow structures and vorticity at *Re* = 500 on the default FLUENT and LB grids.

Located at 0.3*D* from the start of mixing element and at t = 10,000 LB s.

are the 0.7M mesh for FLUENT and the 2.4M grid for LB, respectively. Furthermore, Figure 5 shows that the overall flow structures and axial vorticity, which are obtained on the default grids, match almost perfectly.

Figure 6 shows the pressure drop and Reynolds number at different grid sizes (lefthand side) as well as velocity profiles along a line half way a mixing element (righthand side) at t = 10,000 LB s. The viscosity and body force are set such that a Reynolds number of Re = 500 is obtained. The points to the right are calculated with the LB method, whereas the others are calculated with FLUENT. The pressure drop and Reynolds number can be predicted on the default FLUENT (0.7M) mesh. However, the corresponding velocity profiles show significant differences. It seems that the FLUENT mesh is still not "dense" enough to capture all features of the flow. However, when looking at the overall flow structures and vorticity, which are shown in Figure 7, one can see that the differences are not too large. The velocities obtained on the LB default (7.8M) grid also shows some small differences with those obtained on the more dense grids, but in general they agree well. It should be noted that, although the global geometries match, there can be small differences in the location and time of the LB profiles resulting from the different lattice spacing of the grids and discrete time-step size. Furthermore, LB used far less CPU time than FLUENT. The computational demands of both methods will be discussed in more detail in the next section.

Figure 8 shows the time characteristics of the velocity at a monitoring point that is located close to the center of one of the vortices. In spite of the differences observed in the velocity profiles, there is a good agreement between LB and FLUENT, which are both obtained on the default grids. Even for the longer times we see that the flow oscillations correspond reasonably well. This time-dependent behavior will be explored in more detail in the section "Oscillations in Kenics Static Mixer."

In Figure 9, the normalized pressure drop K as a function of the Reynolds number is plotted for the different grid sizes and is also compared with correlations used in the literature (Bakker and Marshall, 1992; Wilkinson and Cliff, 1977) and experimental data (Mudde et al., 2002). In the literature the normalized pressure drop is usually presented as the ratio between the pressure drop over a static mixer and over an empty tube of equal length, respectively

$$K = \frac{\Delta p_{\text{mixer}}}{\Delta p_{\text{tube}}} \tag{7}$$

For low Reynolds numbers, the results correspond to the correlation from Chemineer (Bakker and Marshall, 1992) and for high Reynolds numbers the results correspond to the correlation from Wilkinson and Cliff (1977). The results are also in good agreement with the experimental data from Mudde et al. (2002). It should be noted, that the L/D ratio of the mixer used by Mudde et al. (2002) was 1.6 instead of 1.5. However, this small difference does not seem to have much influence on the pressure drop. Furthermore, the FLUENT results compare well to the LB results except for the results obtained on the very coarse (15K) mesh, which are slightly off. However, the 15K results could still be good enough for some engineering purposes, which concern only the pressure drop.

Computational demands of LB and FLUENT

Table 1 shows the comparison of the computational demands of FLUENT and LB, respectively. One should note that the steady results are calculated with both the steady and transient solver of FLUENT and that all values related to time are presented in default LB units. For the steady flow at Re = 200, FLUENT can use the steady solver and is roughly two times

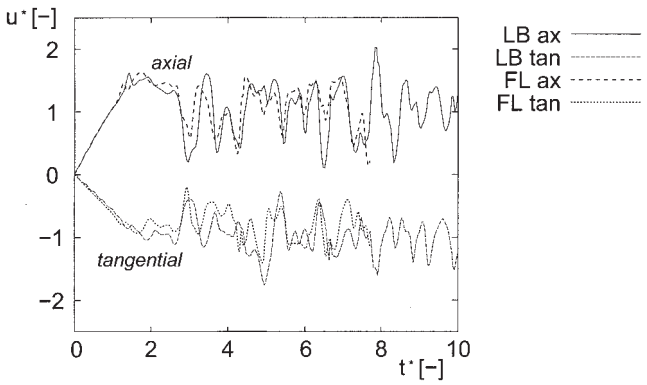

Figure 8. Axial and tangential velocity in monitor point close to the center of a vortex at *Re* = 500.

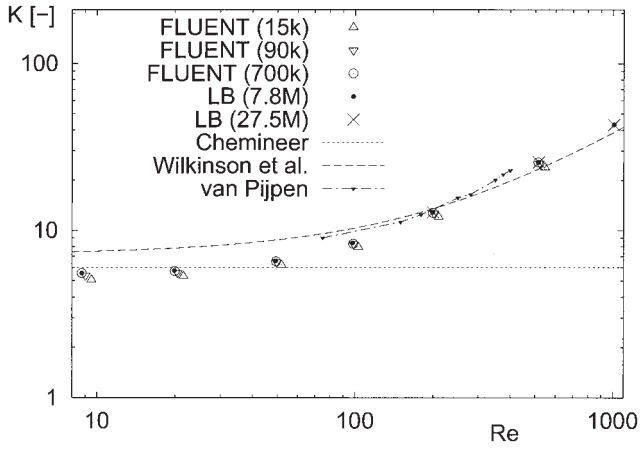

Figure 9. Normalized pressure drop as a function of Reynolds number at different grid sizes.

faster than LB (coarse). When the transient startup ($\mathbf{u} = 0$ at $t = 0$) is simulated at $Re = 200$, FLUENT can use a bigger time step than LB, but still is roughly two times slower than LB (coarse). Because FLUENT has the option to select the steady-state solver, it outperforms LB for the low (steady) Reynolds numbers. It should be noted, however, that the LB method intrinsically solves a time-dependent flow and that the time step is directly linked to the grid spacing.

At $Re = 500$, the flow is unsteady and FLUENT needs a smaller time step than at $Re = 200$, to capture the oscillations that occur in the flow. As a result the computational time that FLUENT needs at $Re = 500$ increases dramatically. FLUENT now is about five times slower than LB, which makes the LB method, especially for this range, a good alternative.

The memory usages of both methods are of a different order. FLUENT uses roughly about four times more memory per grid cell than LB uses per grid node. LB uses about 165 bytes per grid node, but about 22% of the nodes are unused wall nodes, which also consume memory. Taking this into account, LB uses effectively about 215 bytes per used grid node, whereas FLUENT uses about 990 bytes per grid cell. Another disadvantage of an iterative solver like FLUENT is the dramatic increase of CPU time, when the grid is refined, which makes FLUENT slow at dense grids. However, the LB method also has one drawback. Because of the staircase grid, LB minimally needs about 2.4M grid nodes to correctly describe the walls of the Kenics static mixer. Therefore, the LB method is most effective, when a dense mesh is required for the flow structures as well.

Laser Doppler Anemometry

Experimental setup

The setup consists of a 12 element Kenics static mixer, which is composed of stainless steel and is coated black to reduce reflections. The flow in the Kenics mixer is fully developed after about three or four mixing elements and the developed flow is comparable to the flow in the four-element periodic mixer, which is in fact an infinitely long mixer. The aspect ratios of the "experimental" static mixer are $L/D = 1.6$ and $t/D = 0.083$ and the length and diameter of the mixing elements are $L_0 = 76.5 \pm 1$ mm and $D_0 = 48.0 \pm 1$ mm, respectively. The LB simulations are adjusted to match this geometry. Furthermore, the measurement section is made optically accessible by a Perspex tube and is surrounded by a square box with glass windows in it to reduce refraction.

The accuracy of LDA measurements is better at higher velocities. Therefore, a glycerol/water solution is used to increase the viscosity to be able to increase the velocity (while keeping the Reynolds number constant). This results in a smaller uncertainty in the LDA measurements at the relatively low Reynolds numbers. The flow is gravity driven to ensure a constant flow-rate. Furthermore, a feedback system is used to control the temperature by a heating and cooling unit. The temperature is kept constant with an accuracy of 0.1°C and the Reynolds number is set by varying the viscosity and velocity (Re = 20, 50, 100, . . . , 450, 500). The flow rate is measured with a rotameter, which is calibrated for each viscosity with an integrated mass-flow calibration system. The calibration method was tested with LDA measurements in an empty tube.

A dual-beam 4W (Ar^+) laser is used and the light is transmitted by a 2-D probe in back-scatter mode, which allows simultaneous measurement of both the axial and tangential velocity component in a measurement volume. The measurement volume is formed by the intersection of the beams. The velocity components are measured by detecting the back-scattered light of seeding particles, which are added to the flow and consist of glass hollow spheres. These particles are neutrally buoyant and have a diameter in the order of 10 μm. The data are preprocessed by the IFA 750 processor and stored on a normal desktop PC. The data rate was about 50–300 Hz. In

Table 1. Comparison of LB and FLUENT with Respect to CPU Time and Memory at $t = 10{,}000$ LB s (in Default LB Units)

Solver	Grid Size (M)	Time-Step Size (LB s)	Number of Time Steps	CPUs	Memory (MB)	CPU Time (h)
			Re = 200 (steady)			
FLUENT (unsteady)	0.7	100	100	4	660	4.5
FLUENT (steady)*	0.7	∞	1	4	660	1.3
LB (coarse)**	2.4	1.5	6667	4	490	2.3
LB (default)	7.8	1	10000	4	1600	12
			Re = 500 (unsteady)			
FLUENT (unsteady)	0.7	10	1000	4	660	62
LB	7.8	1	10000	4	1600	12

*The steady-state solver of FLUENT was selected.
**Because the grid spacing is bigger, the time step is larger.

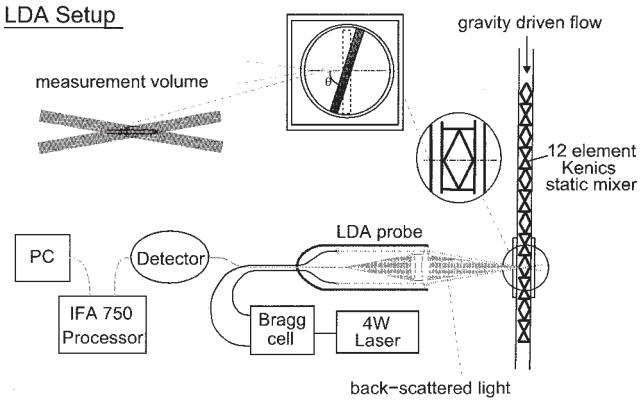

Figure 10. LDA setup and location of measurement volume.

Figure 10 an overview of the setup and measurement location is given.

After processing the raw data two velocity time series are obtained of the axial and tangential velocity components, respectively. The time between data (time between two data points) distribution was Poisson distributed, which is normal for LDA data. [A deviation from the Poisson distribution usually is an indication of an error source (van Maanen, 1999).] The data were resampled using sample and hold to calculate the spectra with the FFT. For the resample frequency the average data rate was used. Profiles are measured halfway along a mixing element in a developed flow.

Velocity profiles

The static mixer is at an angle of $\theta = 65°$ with respect to the center line of the laser beams (see Figure 10). When this angle is taken into account, the LB and LDA velocity profiles match for all Reynolds numbers which are measured (see Figures 11 and 12). The alignment error in the radial position is in the order of 1.5 mm, which is about 3% of the tube diameter. The error in the dimensionless velocity was at most 0.01. At $Re = 500$ (Figure 12) the dimensionless mean velocity and standard deviation are plotted. The mean velocity of the LB simulation was obtained between $t = 18{,}000$ LB s and $t = 20{,}000$ LB s. The relatively large standard deviation at $Re = 500$ is mainly caused by the unsteady flow in the form of the oscillation of vortices and compares quite well to the LB simulations. However, near the wall a deviation is found in the tangential component. This deviation is absent in the axial component. Unfortunately, a satisfactory explanation for this deviation could not be found.

Oscillations in Kenics Static Mixer

Dynamic behavior

The dynamic behavior of the flow in the Kenics static mixer is investigated by looking at the power spectra. The power spectra are obtained from the times series, which are measured (LDA) or simulated (LB) in a monitor point. The monitor point is located at the middle of the velocity profiles, which were measured with LDA. At this location the noise, which is caused by scattering light, was minimal and the fluctuations in the velocity were significant. The time series, which were obtained at this point, are made dimensionless with respect to the time $t^* = t\bar{u}_{ax}/D$ and velocity $u^* = u/\bar{u}_{ax}$. The dimensionless time series are split into a number of blocks (55 for LDA, 57 for LB, and 7 blocks for FLUENT). The blocks have a 50% overlap. For each block the FFT is taken and the spectra are summed and averaged. It should be noted that the LDA and LB results

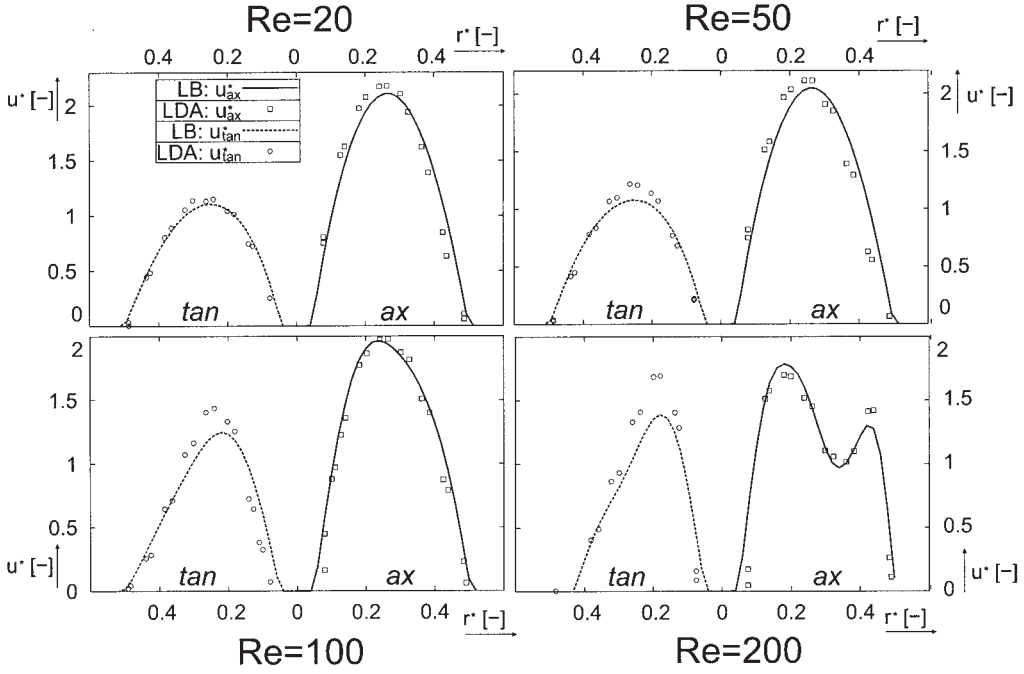

Figure 11. Comparison of velocity profiles obtained with LDA and LB at *Re* values of 20, 50, 100, and 200.

$Re = 20 \cdots 100$: $\eta_0 = 0.070$ Pa·s, $\rho_0 = 1212$ kg/m^3; $Re = 200$: $\eta_0 = 0.0385$ Pa·s, $\rho_0 = 1208$ kg/m^3.

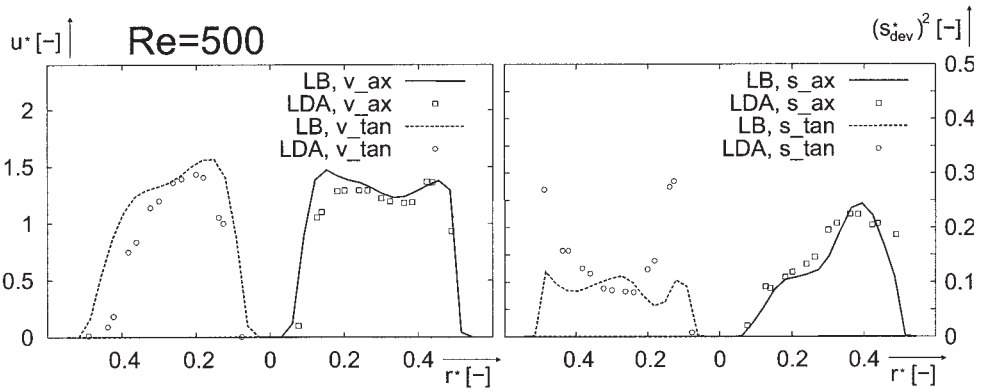

Figure 12. Comparison of velocity profiles (left figure) and standard deviation (right figure) obtained with LDA and LB at *Re* = 500.

$\eta_0 = 0.0275$ Pa·s, $\rho_0 = 1194$ kg/m^3.

were more accurate than the FLUENT results, given that more blocks are used to obtain the spectra.

The power spectra of LDA, LB, and FLUENT, which are normalized by the highest power, are compared at $Re = 500$ (axial component) (see Figure 13). The spectra of LDA and LB show good agreement for the low frequencies and also the slope, which starts around $f^* = 1$, is predicted well. However, there is a deviation at the high frequencies, which is caused by the fact that high frequencies are not fully resolved by LDA because of noise and the resampling of the data (van Maanen, 1999). The spectra of LB and FLUENT show good agreement for the high frequencies at which the slopes match. However, there is a small deviation at lower frequencies, which is probably caused by the low accuracy of the FLUENT spectrum. The FLUENT time series (t_{tot} = 20K LB s) are much shorter than the LB time series (t_{tot} = 300K LB s). And as a result the FLUENT time series can be divided only into seven blocks, which causes a low accuracy of the FLUENT spectrum. The reason for the short FLUENT time series is the long computational time. A simulation of 300K LB s would take 10 weeks with FLUENT and takes only 2 weeks with LB (on four CPUs). Therefore, a shorter time series was used for FLUENT.

The transition from steady to unsteady is investigated experimentally with LDA. The transition is found around $Re = 300$ (see Figure 14). The spectra, which are obtained at $Re \leq 250$, consist only of noise because the flow is steady at this range. When the Reynolds number is increased to $Re = 300$, an oscillation starts to appear, which proves to have a frequency peak around $f^* = 2$. This frequency is observed in both the axial and tangential component and corresponds to a length scale ($1/k$) of roughly half a diameter ($1/k = D/f^*$), which is the largest length scale in the radial direction (the mixer cuts the tube in half). When the Reynolds number is increased further to $Re = 350$, the oscillation becomes irregular, which results in an uniform spectrum up to $f^* = 1$, after which the spectrum drops. The uniform part of the spectrum corresponds to scales larger than the length of a mixing element ($f^* < 0.67$) and are likely a results of the periodicity of the "Kenics static mixer." The nonuniform part of the spectrum corresponds to the scales smaller than the tube diameter, which are caused by the irregular oscillation of the vortices. This behavior is also observed at higher Reynolds numbers up to $Re = 500$ (see Figure 15). Furthermore, the relative power of the small scales (that is, smaller than the tube diameter) increases as the Reynolds number increases.

Figure 16 shows the autocorrelation function at $Re = 300$ and $Re = 500$ of the LB and LDA dimensionless time series, respectively. At $Re = 300$ both LB and LDA show a periodic signal, but the frequency differs (LB: $f^* = 1$ and LDA: $f^* = 1.75$). One should note that correlation of the LDA time series

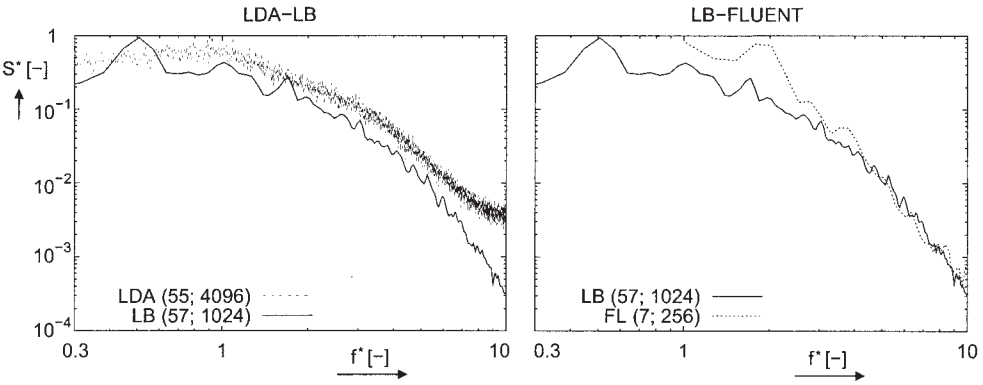

Figure 13. *Re* = 500: Comparison (normalized) power spectra of LDA to LB and LB to FLUENT.

Numbers between brackets indicate: (number of blocks; block size).

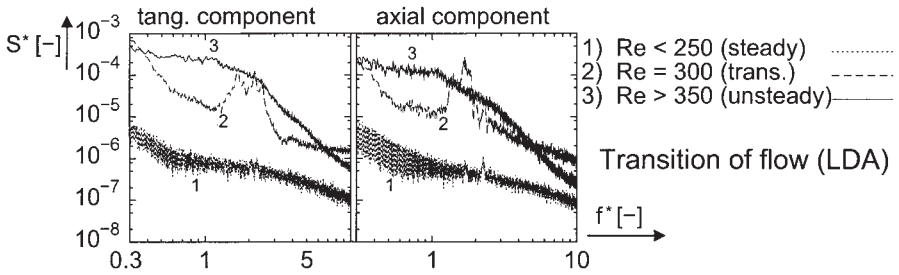

Figure 14. Power spectra indicate transition from steady to unsteady (LDA).

is lower because of uncorrelated noise, which affects the LDA data. The difference in frequency might be caused by the periodicity of the LB geometry. The static mixer used in the LDA setup consists of 12 elements, whereas the one used in the LB simulation is periodic over four elements. Therefore, the frequency, which is found in the LDA time series, might be influenced by the entrance and exit effects of the static mixer. A longer mixer might be necessary to capture the right transition with the LDA experiments. At $Re = 500$ the autocorrelation functions of LDA and LB both show that there is almost no correlation. Again, the lower correlation of the LDA time series is caused by the uncorrelated noise, which is absent in the LB simulation. Taking this into account, the autocorrelation functions of LDA and LB agree reasonably well. So, it seems that for the irregular fluctuations in the velocity at $Re = 500$ the periodicity of the mixer is less important.

Flow in Kenics static mixer at different Re values

The early transition to unsteady flow at $Re = 300$ can be explained by looking at the vortical structures, which are formed in a mixing element of the Kenics static mixer (see Figure 17). At the low Reynolds numbers ($Re \leq 200$) the vortical structures end within one mixing element and the flow aligns with the twist of the element before it reaches the next mixing element, which results in a steady flow. At higher Reynolds numbers ($Re > 300$) the vortical structures stretch out along the entire length of a mixing element and the flow no longer has time to align with the mixing element. As a result the vortical structures create a disturbance at the intersection of two mixing elements, which triggers the unsteady behavior.

This unsteady behavior is visualized for $Re = 500$ and $Re = 1000$ as a function of time (in LB s) (see Figure 18). Five snapshots are shown. The first snapshot shows a developed flow ($t = 0$ LB s) and the others, the progression of the flow in time (up to $t = 100$ LB s). Although the fluctuations in a point can be significant, they do not seem to influence the overall structures of the flow. The vortices oscillate slightly, but they are stable at $Re = 500$ and the flow is still symmetric. At $Re = 1000$, however, the flow becomes more unsteady and is no longer symmetric. Vortices merge with one another and the overall flow pattern seems to constantly change. Although large structures remain dominant, smaller structures appear and disappear over time. The flow seems to become turbulent at Re = 1000, but no cascade process of vortices, which break up into smaller vortices, can be observed.

Discussion and Conclusions

A good agreement between the results obtained with LB, FLUENT, and LDA measurements, regarding the velocity field and its time characteristics, was obtained.

At low Reynolds numbers the flow is steady and FLUENT was more efficient than LB. At $Re = 200$ FLUENT is about two times faster than LB. This is mainly because FLUENT can use the steady-state solver together with a coarser grid. The time step in LB is connected with the lattice spacing. Because the boundaries at the wall in LB are staircased, a relatively dense grid is required to accurately resolve the flow in complex geometries. More sophisticated methods to deal with the wall are currently being studied (Bouzidi et al., 2001; Chen et al., 1998; Rohde et al., 2002; Verberg and Ladd, 2002). Besides that, LB is intrinsically an unsteady solver, which has to converge to the steady solution. Formulation of steady LB solvers is currently still a research topic (Bernaschi and Succi, 2003).

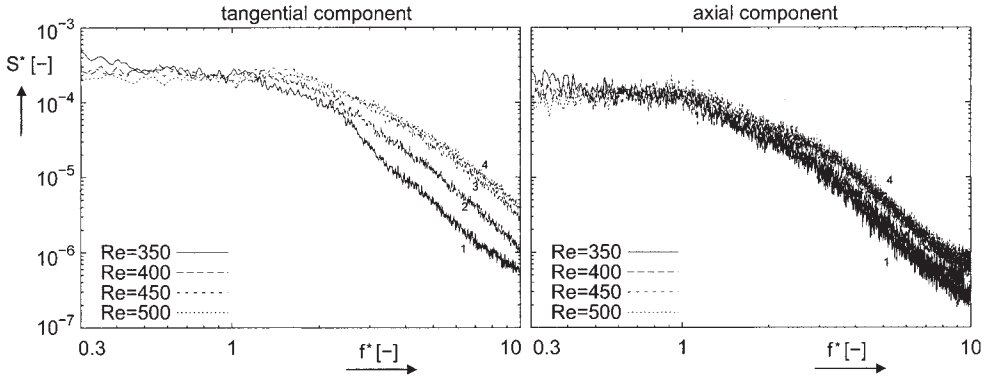

Figure 15. Power spectra of unsteady flow in Kenics static mixer at *Re* > 350 (LDA).

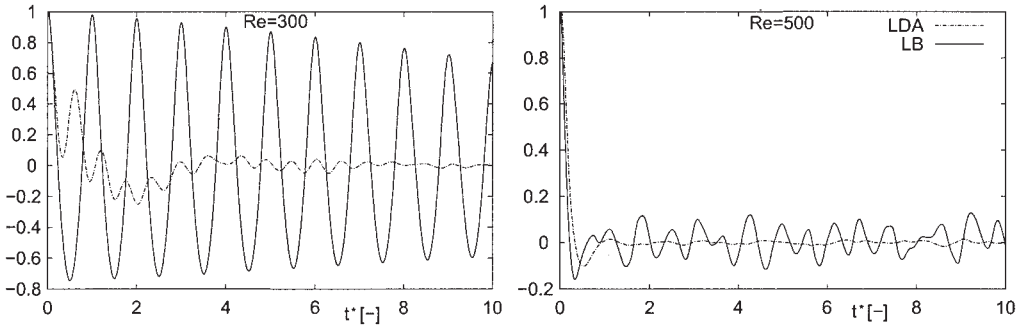

Figure 16. Autocorrelation function of LB and LDA time series at *Re* = 300 and *Re* = 500.

At the higher (transient) Reynolds numbers the picture changes. Small-scale structures (vortices) appear in the flow, which require a more dense grid and the use of a smaller time step. FLUENT then also needs a small time step to capture the oscillations, which leads to a rather long computational time. In this case, FLUENT is about five times slower than LB. LB has a high spatial resolution and small time step at low computational cost, which makes it a promising tool to study the dynamic behavior in transitional flows. It should be noted that FLUENT is a generic-purpose code, whereas the LB code was specifically designed and optimized for this range.

The CFD results were validated by LDA experiments. The velocity profiles as well as the power spectra agreed quite well. It seems that both the flow and time scales are predicted well by the simulations. Furthermore, the (LDA) power spectra provide us with information about the transition of the flow from steady state to transient flow. The transition takes place around $Re = 300$ and is also found in the simulations at almost the same Reynolds number.

Although good agreement was found between the CFD results and the LDA data, one should note that the comparison with LDA was made along a single line, which is located halfway along a mixing element (Figure 10). The results of the simulations indicate that the most critical part of the flow might be located at the intersection of two elements. Experimental data in this area would be helpful to provide us with a more rigorous test to validate the CFD results. Therefore, a more detailed LDA or other experimental study into the flow of the Kenics static mixer can be an interesting topic for future research.

The onset of the transient behavior could be explained by the length of the vortices, which stretch out along a mixing element. It seems that when the flow does not have enough time to align with the mixing elements, the vortical structures create a disturbance at the intersection of two mixing elements. This disturbance triggers the transient and chaotic behavior, which

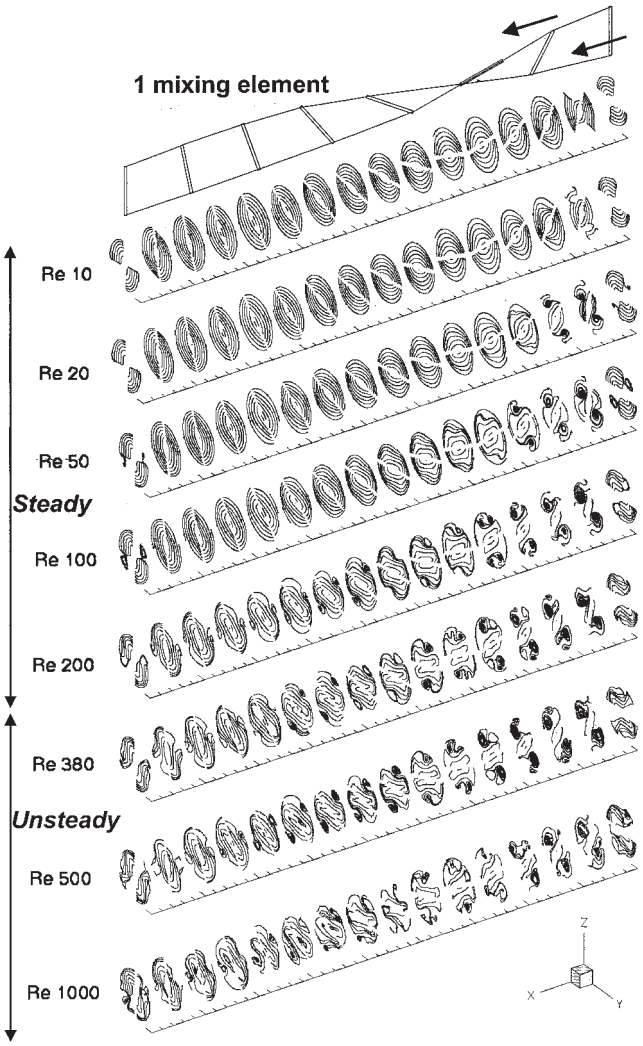

Figure 17. Flow structures in mixing element of Kenics static mixer at different Reynolds numbers visualized by 2-D stream-traces at various planes in mixing element.

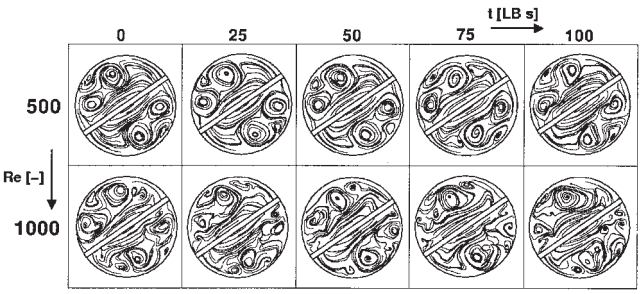

Figure 18. Small oscillations of vortex core at *Re* = 500 and *Re* = 1000 visualized by 2-D stream traces located at 0.3*D* from start of mixing element.

occurs already at a relative low Reynolds number. If the Reynolds number is increased the flow becomes increasingly chaotic and more small vortical structures appear and at Re = 1000 the flow seems to have become turbulent.

The insight, which is gained about the flow in the Kenics static mixer, can be valuable for other studies such as the mixing process of the liquids or solids (particles). A particle tracking code can be implemented into LB code, thus enabling the study of mixing of particles or tracers (van Wageningen et al., 2003). It is also possible to study higher Reynolds number, when LES is incorporated into the lattice Boltzmann solver (Derksen and van den Akker, 1999). Furthermore, multiphase models for LB seem to be ready in the near future (Chen and Doolen, 1998), which opens up the possibility of simulating industrial multiphase flows in static mixers.

Acknowledgments

This research project was funded by the "IOP Heavy Metals," which is a Dutch institution that sponsors new environmental technologies.

Notation

$\mathbf{c}i$ = lattice velocity at link i
D = element or tube diameter, m
F = force, N
f = frequency, Hz
$f(\mathbf{r}, t)$ = particle density at link i
K = normalized pressure drop, —
k = wavenumber, 1/m
L = element length, m
l = length, m
n = number, —
p = pressure, Pa
r = radial direction, m
$\mathbf{r}$ = lattice point
S = power of spectra, —
s = standard deviation, *
t = element (blade) thickness, m
t = time, s
t = lattice time step
u = velocity, m/s
x = (axial) x-coordinate, m

Greek letters

η = viscosity, Pa·s
ρ = density, kg/m^3
τ = BGK relaxation parameter

Dimensionless number

Re = Reynolds number based on D

Subscripts

ax = axial
b = body
nodes = grid nodes
i = lattice link
mixer = tube with static mixer
rad = radial
tan = tangential
tot = total (time)
tube = tube without static mixer

Superscripts

* = dimensionless
eq = equilibrium

Acronyms

CFD = Computational Fluid Dynamics
FE = finite element
FL = FLUENT
FV = finite volume
LB = lattice Boltzmann
LDA = laser Doppler anemometry

Literature Cited

Arimond, J., and L. Erwin, "A Simulation of a Motionless Mixer," *Chem. Eng. Commun.*, **37**, 105 (1985).
Bakker, A., and R. LaRoche, "Flow and Mixing with Kenics Static Mixers," *Chem. Eng. Commun.*, **136**, 119 (1995).
Bakker, A., and E. M. Marshall, "Laminar Mixing with Kenics In-Line Mixers," Proc. of Fluent Inc.'s 1992 Users Group Meeting, Burlington, VT (1992).
Bernaschi, M., and S. Succi, "Accelerated Lattice Boltzmann Scheme for Steady-State Flows," *Int. J. Mod. Phys. B*, **17**, 1 (2003).
Bouzidi, M., M. Firdaouss, and P. Lallemand, "Momentum Transfer of a Boltzmann-Lattice Fluid with Boundaries," *Phys. Fluids*, **13**(11), 3452 (2001).
Chen, H. D., C. Teixeira, and K. Molvig, "Realization of Fluid Boundary Conditions via Discrete Boltzmann Dynamics," *Int. J. Mod. Phys. C*, **9**(8), 1281 (1998).
Chen, S., and G. D. Doolen, "Lattice Boltzmann Method for Fluid Flows," *Annu. Rev. Fluid Mech.*, **30**, 329 (1998).
Chen, S. J., and A. R. MacDonald, "Motionless Mixers for Viscous Polymers," *Chem. Eng.*, 105 (1973).
Cybulski, A., and K. Werner, "Static Mixers Criteria for Applications and Selection," *Int. Chem. Eng.*, **26**, 171 (1986).
Derksen, J. J., and H. E. A. van den Akker, "Large Eddy Simulations on the Flow Driven in a Rushton Turbine," *AIChE J.*, **45**, 209 (1999).
Fluent Inc., *Computerized Flow Modeling for Industry*, Fluent USA, Lebanon, NH (2003a).
Fluent Inc., Fluent 6.1 Documentation (online manual url http://www.fluentusers.com), Fluent USA, Lebanon, NH (2003b).
Fourcade, E., R. Wadley, H. C. J. Hoefsloot, A. Green, and P. D. Iedema, "CFD Calculation of Laminar Striation Thinning in Static Mixer Reactors," *Chem. Eng. Sci.*, **56**, 6729 (2001).
Genetti, W. E., "Laminar Flow Heat Transfer with Inline Mixers," *Chem. Eng. Commun.*, **16**, 325 (1982).
Grace, C. D., "Static Mixing and Heat Transfer," *Chem. Proc. Eng.*, **52**, 57 (1971).
Hage, J. L. T., M. A. Reuter, R. D. Schuiling, and I. S. Ramtahalsing, "Reduction of Copper with Cellulose in an Autoclave; An Alternative to Electrolysis," *Minerals Eng.*, **12**, 393 (1999).
Harnby, N., M. F. Edwards, and A. W. Nienow, *Mixing in the Process Industries*, 2nd Edition, Butterworth–Heinemann, Oxford, UK (1992).
Heywood, N. I., L. J. Viney, and I. W. Stewart, "Mixing Efficiencies and Energy Requirements of Various Motionless Mixer Designs for Laminar Mixing Applications," Proc. of Fluid Mixing II Symposium, Bradford, UK, pp. 147–176 (1984).
Hobbs, D. M., and F. J. Muzzio, "Effects of Injection Location, Flow Ratio, and Geometry on Kenics Mixer Performance," *AIChE J.*, **43**(12), 3121 (1997a).
Hobbs, D. M., and F. J. Muzzio, "The Kenics Static Mixer: A Three-Dimensional Chaotic Flow," *Chem. Eng. J.*, **67**, 153 (1997b).
Hobbs, D. M., and F. J. Muzzio, "Reynolds Number Effects on Laminar Mixing in the Kenics Static Mixer," *Chem. Eng. J.*, **70**, 93 (1998).
Hobbs, D. M., P. D. Swanson, and F. J. Muzzio, "Numerical Characterization of Low Reynolds Number Flow in the Kenics Static Mixer," *Chem. Eng. Sci.*, **53**, 1565 (1998).
Joshi, P., K. D. P. Nigam, and E. B. Nauman, "The Kenics Static Mixer: New Data and Proposed Correlations," *Chem. Eng. J.*, **59**, 265 (1995).
Kandhai, D., D. J. E. Vidal, A. G. Hoekstra, H. Hoefsloot, P. Iedema, and P. M. A. Sloot, "Lattice-Boltzmann and Finite Element Simulations of Fluid Flow in an SMRX Static Mixer Reactor," *Int. J. Numer. Methods Fluids*, **31**, 1019 (1999).
Kemblowski, Z., and P. Pustelnik, "Residence Time Distribution of a Power-Law Fluid in Kenics Static Mixers," *Chem. Eng. Sci.*, **43**, 473 (1988).
Lecjacks, Z., I. Machac, and J. Sir, "Heat Transfer to a Newtonian Liquid

Flowing through a Tube with an Internal Helical Element," *Int. Chem. Eng.*, **27**, 205 (1987).
Mudde, R. F., C. van Pijpen, and R. Beugels, "Simulation of the Laminar Flow in a Primix Static Mixer," *Proc. ASME-PVP*, **448**(2), 67, (2002).
Nigam, K. D. P., and K. Vasudeva, "Residence Time Distribution in Static Mixer," *Can. J. Chem. Eng.*, **58**, 543 (1980).
Ottino, J. M., *The Kinematics of Stretching, Chaos and Transport*, Cambridge Univ. Press, Cambridge, UK (1989).
Pahl, M. H., and E. Muschelknautz, "Static Mixers and Their Applications," *Int. Chem. Eng.*, **22**, 197 (1982).
Qian, Y. H., D. d'Humieres, and P. Lallemand, "Lattice BGK Models for Navier–Stokes Equation," *Europhys. Lett.*, **17**, 479 (1992).
Qian, Y. H., and S. A. Orszag, "Lattice BGK Models for the Navier–Stokes Equation: Nonlinear Deviation in Compressible Regimes," *Europhys. Lett.*, **21**, 225 (1993).
Rauline, D., J. M. Le Blevec, J. Bousquet, and P. A. Tanguy, "A Comparative Assessment of the Performance of the Kenics and SMX Static Mixers," *Trans. IChemE*, **78**, 389 (2000).
Rauline, D., P. A. Tanguy, J. M. Le Blevec, and J. Bousquet, "A Numerical Study on Mixing in the Kenics Static Mixer," *Chem. Eng. Commun.*, **136**, 119 (1995).
Rohde, M., J. J. Derksen, and H. E. A. van den Akker, "Volumetric Method for Calculating the Flow around Moving Objects in Lattice-Boltzmann Schemes," *Phys. Rev. E*, **65**(5), 056701 (2002).
Sir, J., and Z. Lecjacks, "Pressure Drop and Homogenization Efficiency of a Motionless Static Mixer," *Chem. Eng. Commun.*, **16**, 325 (1982).
van Maanen, H. R. E., "Retrieval of Turbulence and Turbulence Properties from Randomly Sampled LDA Data with Noise," PhD Thesis, Delft University of Technology, Delft, The Netherlands (1999).
van Wageningen, W. F. C., R. F. Mudde, and H. E. A. van den Akker, "Numerical Investigation into Mixing of Particle-Laden Flows in a Kenics Static Mixer," Proc. Of 11th European Mixing Conference, Bamberg, Germany, pp. 137–144 (2003).
Verberg, R., and A. J. C. Ladd, "Accuracy and Stability of a Lattice-Boltzmann Model with Subgrid Scale Boundary Conditions," *Phys. Rev. E*, **65**(1), 016701 (2002).
Wilkinson, W. L., and M. J. Cliff, "An Investigation into the Performance of a Static In-Line Mixer," Proc. of 2nd European Conf. on Mixing, Cambridge, UK (1977).

Manuscript received July 9, 2003, and revision received Nov. 28, 2003.